Measurements of charge state distributions of 0.74 and 1.4 MeV/u heavy ions passing through dilute gases

P. Scharrer* and Ch. E. Düllmann

Helmholtz-Institut Mainz, Johannes Gutenberg-Universität Mainz, 55099 Mainz, Germany, GSI Helmholtzzentrum für Schwerionenforschung GmbH, 64291 Darmstadt, Germany; and Johannes Gutenberg-Universität Mainz, 55099 Mainz, Germany

W. Barth, J. Khuyagbaatar, and A. Yakushev

Helmholtz-Institut Mainz, Johannes Gutenberg-Universität Mainz, 55099 Mainz, Germany and GSI Helmholtzzentrum für Schwerionenforschung GmbH, 64291 Darmstadt, Germany

M. Bevcic, P. Gerhard, L. Groening, K. P. Horn, E. Jäger, J. Krier, and H. Vormann

GSI Helmholtzzentrum für Schwerionenforschung GmbH, 64291 Darmstadt, Germany

(Received 9 January 2017; published 24 April 2017)

In many modern heavy-ion accelerator facilities, gas strippers are used to increase the projectile charge state for improving the acceleration efficiency of ion beams to higher energies. For this application, the knowledge on the behavior of charge state distributions of heavy-ions after passing through dilute gases is of special interest. Charge state distributions of uranium (^{238}U), bismuth (^{209}Bi), titanium (^{50}Ti), and argon (^{40}Ar) ion beams with energies of 0.74 MeV/u and 1.4 MeV/u after passing through hydrogen (H_2), helium (He), carbon dioxide (CO_2), nitrogen (N_2), oxygen (O_2), neon (Ne), and argon (Ar) gases were measured. Gas stripper target thicknesses up to 100 $\mu g/cm^2$ were applied. The observed behavior of the charge state distributions, including their width and mean charge state, are discussed. The measurements show the highest equilibrium charge state at 1.4 MeV/u for ^{238}U on H_2 gas of 29.2 ± 1.2. Narrow charge state distributions are observed for ^{238}U and ^{209}Bi on H_2 and He gas, which are highly beneficial, e.g., for the production of beams of high intensities in accelerators.

DOI: 10.1103/PhysRevAccelBeams.20.043503

I. INTRODUCTION

Charge stripping is a key technology for heavy-ion accelerator facilities, as the output charge state, the efficiency to produce ions in the selected charge state, and the beam quality after stripping are directly effecting the performance of the accelerator. Therefore, the charge state distribution of heavy ions passing through matter is of special interest in heavy-ion accelerator physics. Many modern accelerator facilities such as the Radioisotope Beam Factory (RIBF) at RIKEN, Wako, Japan [1], the future Facility for Rare Isotope Beams (FRIB) at MSU, East Lansing, MI, USA [2], the High Intensity heavy ion Accelerator Facility (HIAF) at HIRFL, Lanzhou, China [3], and the future Facility for Antiproton and Ion Research (FAIR) at GSI, Darmstadt, Germany [4], aim at providing high-intensity, heavy-ion beams with energies beyond 200 MeV/u. For the acceleration of high-intensity heavy ions to such energies, ions generated in an ion source at comparatively low charge states are initially accelerated only to a few MeV/u. They are then guided to a charge stripper, where they pass through matter of a target to increase the average charge state of the ions in charge-exchanging collisions between the ions and the atoms or molecules of the target. Behind the charge stripper, one or several ion charge states are selected for further acceleration. This enables a more efficient acceleration up to the final beam energy, compared to acceleration of ions with a lower charge state.

For charge stripping of high-intensity heavy-ion beams, using gas targets is usually preferred to using solid targets. Heavy ions, like U, have a significantly larger energy deposition per unit length than light projectiles. For example, the energy deposition of an ^{238}U ion at 1.4 MeV/u in a C-foil is about 27 MeV/μm, while a proton with the same energy deposits only about 0.041 MeV/μm [5]. The much higher energy deposition of heavy-ion beams significantly increases radiation damage in solids and also leads to thermal effects in the target [6]. In addition, such beams can induce density variations in solid target foils, which may result in an increased energy spread of the beam. Altogether, this can result in the destruction of the foil (see, e.g., [6]). In contrast, gas targets have a practically infinite lifetime. However, the use of gas

*p.scharrer@gsi.de

targets generally results in comparatively lower average charge states, due to the reduced density in gases compared to solid materials [7].

The charge state distribution of heavy ions passing through gases is governed by charge-exchanging collisions between ions and gas particles. Many theoretical and experimental investigations of charge-exchanging processes have been performed, starting already decades ago [8,9]. These processes are divided into electron-loss and electron-capture depending on the change of the charge state of the ion traveling through the gas. As a result of a sequence of charge-exchanging collisions, the ion charge state approaches a state of dynamic equilibrium around a mean charge state, depending on the ion energy, the ion type, as well as the target type and density [9]. In this equilibrium, the number of electron-capture processes equals the number of electron-loss processes per unit pathlength on average. The mean charge state of the resulting equilibrium charge state distribution, which is independent on the initial charge state of the ions, is the so-called "equilibrium charge state." The charge state distribution is of special interest in charge strippers for accelerator facilities, as it relates to a maximum achievable charge state and beam intensity behind the stripper, using a certain ion-target combination at a fixed ion energy. Because of this, the gas target and the applied target density are a key for improving the charge stripper performance.

Despite their importance for accelerator performance, experimental data on the charge state distribution of heavy-ions for particular beam parameters and gases are surprisingly scarce. This may be due to the large number of combinations for ion projectiles, target media, and relevant parameters for the stripping process, e.g., beam energy and target density.

The GSI Universal Linear Accelerator (UNILAC) [10] is a heavy-ion accelerator with a maximum output ion energy of 11.4 MeV/u. A modified setup for the gas stripper at 1.4 MeV/u ion energy was recently developed, in the context of an UNILAC upgrade program toward the future FAIR facility [11]. The previously existing gas stripper is based on a continuous N_2 gas-jet. In the new setup, this was replaced by a pulsed gas stripper cell, exploiting the low duty cycle operation of FAIR ($\leq$200 μs-long beam pulses, $\leq$3 Hz repetition rate) [12]. The gas injection is synchronized with the pulsed timing of the accelerator. Thanks to the low duty cycle, the effective gas load for the differential pumping system is significantly reduced compared to the N_2 gas-jet based setup. Thus, it is possible to increase the effective gas density for the stripping process significantly, without exceeding the limitations of the pumping system. The increased gas densities allow for using low-Z targets, like H_2 and He, which were presumed to be promising stripper targets based on theoretical predictions [13] and similar measurements at higher beam energies at RIKEN [14]. Their use was strongly limited before due to the high gas load of the jet-based gas injection [15]. In recent measurement campaigns applying the new setup, charge state distributions of ^{238}U, ^{209}Bi, ^{50}Ti, and ^{40}Ar ion beams after passing through different gas targets, including H_2 and He, were measured at two different beam energies (0.74 MeV/u and 1.4 MeV/u) [15–19].

II. EXPERIMENTAL SETUP

The GSI UNILAC is able to accelerate ion beams from a wide range of elements, up to ^{238}U, bunched in beam pulses of $\sim$20 μs to 5 ms duration at repetition frequencies of up to 50 Hz. The ion beams are delivered by one of several available ion sources [20]. For this measurement campaign high-intensity U-beams from a Vacuum ARc Ion Source (VARIS) [21] were used. A Penning ionization gauge was used for Bi- and Ti-beam operation. The ion beams are accelerated in the high current injector (HSI) [22] up to 1.4 MeV/u ($\beta = 0.054$) before they reach the gas stripper section [23]. The HSI mainly comprises a radio-frequency quadrupole (RFQ) and two inter-digital H-mode accelerating cavities. The short-pulsed ion beams require high gas densities to be present only during transit through the stripper. Using a pulsed gas injection enables increased stripper target densities and, therefore, the use of low-Z gas targets. With this, measurements over a wide range of target thicknesses up to 100 μg/cm^2 can be performed.

A. Gas stripper

The GSI UNILAC gas stripper section is shown in Fig. 1. The ion beam is focused by two quadrupole doublets and a dipole magnet onto a horizontal analyzing slit (Slit 2), positioned in the charge state separation system behind the gas stripper, to enable for an optimal separation [10]. In front of the gas stripper a beam transformer (Beam transformer 1 in Fig. 1) enables the measurement of the beam current before stripping. In the gas stripper the average charge state of the beam ions is increased due to the charge-changing processes occurring in collisions between ion projectiles and gas particles.

A schematic view of the GSI UNILAC gas stripper is shown in Fig. 2. The gas inlet is mounted on a flange on top of the main stripper chamber. A roots vacuum pump (pumping performance: 2222 l/s) is mounted at the bottom of the main chamber. The adjacent chambers are each connected to a turbomolecular pump (pumping performance: 1200 l/s). Together with additional vacuum pumps in the adjacent beam line, they compose a four-stage differential pumping system to maintain the required vacuum conditions ($<10^{-3}$ Pa).

Two pulsed gas valves are used as a gas inlet, diverted from their intended use in automotive applications. Their opening time can be adapted from a few microseconds up to several milliseconds at repetition frequencies up to 10 kHz. The valves are mounted on top and at the bottom

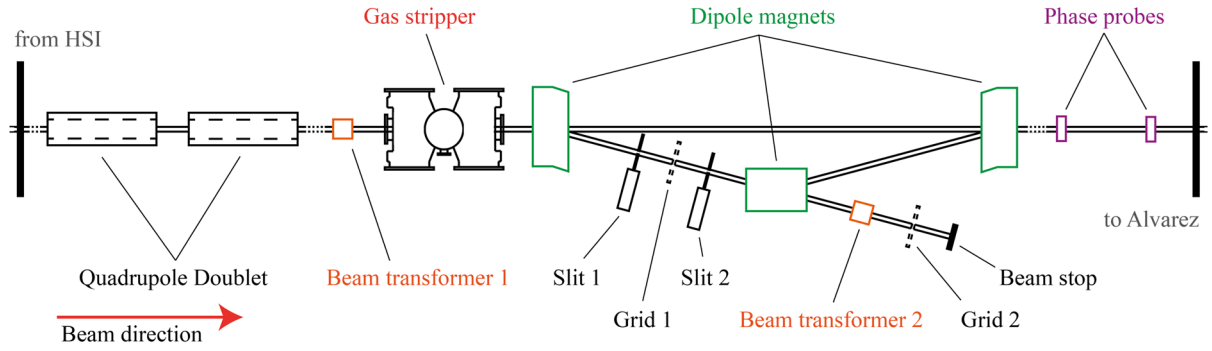

FIG. 1. Schematic of the gas stripper section at the GSI UNILAC: The charge state separation is achieved using a system of three dipole magnets. The ion beams are horizontally focused through the stripper by two quadrupole doublets onto the second analysing slit (Slit 2) behind the first dipole magnet. The beam current can be measured by several beam transformers along the beam line. The beam energy is measured with time-of-flight measurements using phase probes.

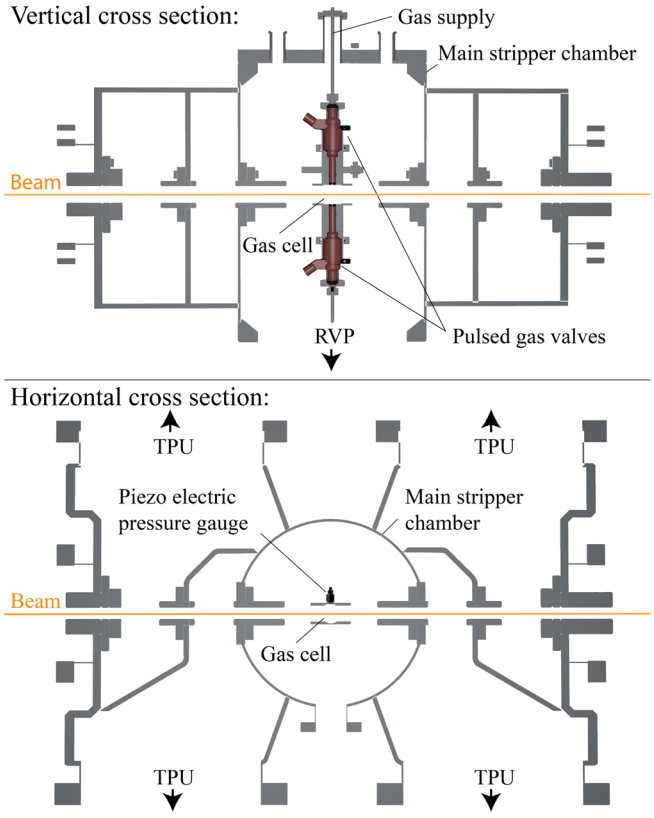

FIG. 2. Schematic cross-sectional views of the main gas-stripper section: (a) vertical and (b) horizontal. The gas cell for the stripping process is fed by two pulsed gas valves (red) positioned on top and on the bottom of the beam line in the main stripper chamber, which are supplied through the top flange. A four-stage differential pumping system is used, comprising a roots vacuum pump (RVP) below the main stripper chamber and four turbomolecular pumps (TPU) on the sides of the adjacent chambers. A piezoelectric pressure gauge is attached to the side of the gas cell to enable pressure measurements.

of the beam line with the gas outlets pointing at each other (see Fig. 2, top). A more detailed view of the core setup is shown in [18]. The gas outlet of both valves is slightly tilted against the beam direction (approximately 10° from the vertical axis). A cross-fitting is used to hold both valves. This arrangement creates a windowless gas cell with high target density. The tube-shaped, enclosed interaction zone is 44 mm long in beam direction with a diameter of 22 mm. For high-intensity ^{238}U beam operation, the beam diameter fills the whole aperture of the stripper-chamber orifices. In this case, the beam diameter at the gas injection is approximately 20 mm. A piezoelectric pressure gauge is mounted at the side of the gas cell to enable pressure measurements.

The opening of the gas valves is controlled by a customized power supply, including a timing option for the control signal. Both valves are controlled separately to be used in combination or independent from each other. The trigger signal for the opening of the valves is generated by a fixed time delay to an artificial timing signal from the accelerator main control unit, indicating the exact time of the beam pulse transit through the stripper.

A separate gas supply for each valve enables for high flexibility in beam operation at the UNILAC [24]. The gas-supply system before the stripper can be evacuated by a piston pump. In between operation with different gas types the gas system is repeatedly evacuated to about 1×10^{-2} hPa, then flushed with the gas to be used, to ensure the purity of the applied gas. Gases of high purity were used (99.999% for H_2, 99.996% for He, 99.5% for CO_2, 99.999% for N_2, 99.999% for O_2, 99.99% for Ne, and 99.998% for Ar).

The valves open shortly before a beam pulse enters the gas stripper to ensure the maximum gas density for the stripping process and close directly after to keep the effective gas load as low as possible. This time offset depends on the applied back-pressure and the gas type. For

higher back-pressures, the maximum gas density in the interaction zone is reached faster. For this measurements, an offset of 300 μs was chosen, which was found to provide sufficient time to reach a maximum gas density for the different gas types in the applied back-pressure range. The total opening time of the valves is set to 400 μs for the 100 μs-long beam pulses for all ion projectiles. A repetition frequency of 1 Hz was applied for all measurements.

B. Charge state separation

After passing the gas stripper, the charge state of the ions is distributed over a wide range. For charge state separation behind the stripper, a system of three dipole magnets is used in combination with two slits between the first and the second magnet (see Fig. 1). In the first dipole magnet, the ions are separated according to their magnetic rigidity:

$$B\rho = mv/qe. \tag{1}$$

B denotes the magnetic flux density, ρ the radius of curvature of the ion trajectory, and m and v are the mass and velocity of the ion, respectively. q is the charge state of the ion and e is the elementary charge. At the present beam energies the magnetic rigidity is written in a relativistic way as

$$B\rho = 3.1071\ \text{Tm} \cdot \frac{A}{q} \cdot (\beta\gamma), \tag{2}$$

with

$$\gamma = \frac{1}{\sqrt{1-\beta^2}} \tag{3}$$

and $\beta = v/c$, where A denotes the atomic mass number of the ion. The nominal deflection angle of the first dipole magnet to the subsequent beam line is 15°. The magnetic field of the dipole magnet can be adjusted to deflect ions up to a maximum magnetic rigidity of 1.98 Tm. This corresponds to $A/q \leq 11.5$ at 1.4 MeV/u. Therefore, the deflection of heavy ions is limited to those having a minimum threshold charge state, depending on the mass of the ions. The magnetic field is too weak to sufficiently bend ions with lower charge states.

The setup for the charge state separation and the measurements of the charge state fractions can be seen in Fig. 1. Behind the first dipole magnet, two slits (Slit 1 and 2) are used to select ions with a specific charge state. Slit 1 gradually reduces the beam load on Slit 2. The width of Slit 2 is adjusted to match the full width of the chosen charge peak. For this, grid measurements on both sides of the slits are used to obtain the width of the charge peak. This concept is shown in Fig. 3 by grid measurements using an ^{238}U beam. Ions with the same charge state have an intrinsic horizontal width due to the horizontal beam emittance, which is also affected by the energy and angular spread from collisions in the stripper target. The separation of $^{238}U^{28+}$ ions by the analysing slit is indicated in Fig. 3(a). On the grid behind the analyzing slits, only ions with the selected charge state are observed. The slit width is typically adjusted in the range of 3–8 mm, depending on the type of ion and gas, the selected charge state, the beam current, as well as the target density. The beam current of ions with the selected charge state is measured behind the second dipole magnet using Beam transformer 2 (see Fig. 1).

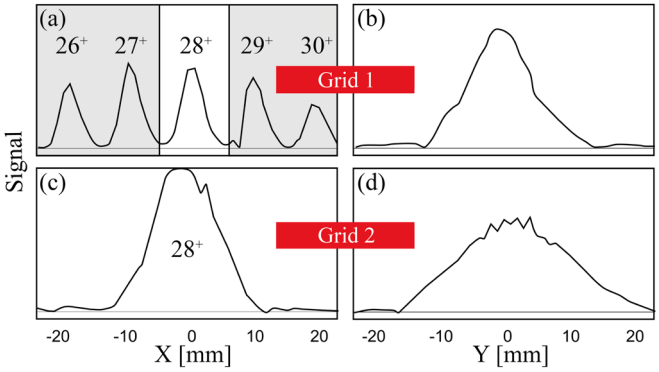

FIG. 3. High-current grid measurements of an ^{238}U beam before (top) and after (bottom) passing Slit 2 (see Fig. 1) in horizontal (left) and vertical (right) plane. The desired charge peak is selected by adjusting the width of the slit, as indicated in panel (a) [16].

The stripping efficiency η_{q_i} into the charge state q_i is calculated using

$$\eta_{q_i} = \frac{I_{q_i}/q_i}{I_{q_{\text{ini}}}/q_{\text{ini}}}, \tag{4}$$

where $I_{q_{\text{ini}}}$ denotes the current of the ions with the initial charge state q_{ini} in front of the stripper and I_{q_i} the current of the ions for charge state q_i behind the charge state separation. During the measurements it was confirmed, that for optimal charge state separation the measured total efficiency $\sum_i \eta_{q_i}$ through the stripper is 100%, within the error range of ±4%. In some measurements not all major-populated charge states could be measured, e.g., due to limitations of the magnetic field of the dipole magnet for heavy-ion beams, as mentioned above. This leads to a reduced apparent beam transmission. Additionally, a systematic effect was observed during the measurements, and is described in Sec. III. To obtain the fraction F_q of the charge state q, the stripping efficiencies are therefore normalized:

$$F_{q_i} = \frac{\eta_{q_i}}{\sum_i \eta_{q_i}}. \tag{5}$$

The charge state distribution can be obtained by plotting the charge state fractions as a function of the corresponding charge state. In case not all charge states could be measured, the missing efficiencies were estimated by

applying a fit to the measurement data as described in detail in Sec. III.

C. Target thickness calibration

The gas density inside the stripper is changed by adjusting the back-pressure on the gas valves. During the measurement campaign, both valves were used separately or in combination, as described in Sec. II A. For each set of valve combination and back-pressure the beam-energy loss through the stripper was measured.

For this, the beam energy was measured by time-of-flight measurements using pairs of adjacent phase probes along the beam line [22]. In these measurements the beam is directed in a straight line without separation of charge state, with the first dipole magnet switched off. From the measured time-of-flight t_{TOF} the velocity v of the ion beam is calculated using $v = Y/t_{\mathrm{TOF}}$, where Y is the distance between the probes. The kinetic energy E of the beam is then calculated from

$$E = 931.4941\ \mathrm{MeV} \cdot A \cdot (\gamma - 1). \tag{6}$$

The distance between the two phase probes is 1630.12 mm. To measure the energy-loss through the gas stripper, the beam energy is measured by the two phase probes behind the stripper (see Fig. 1) both with and without running gas injection.

In Fig. 4(a), the deduced energy loss is depicted exemplary for ^{50}Ti on H_2 at 1.4 MeV/u, using both gas valves simultaneously. The error bars show the estimated uncertainties for the measurement of the beam energy (± 5 keV/u). The energy-loss is increasing linearly within the measured back-pressure range.

The thickness of the gas target was estimated with the SRIM2013 computer code [5] by using the energy-loss measurements, taking into account the ion energy as well as the type of ion projectile and target. This is depicted in Fig. 4(b) for ^{238}U, ^{50}Ti, and ^{40}Ar ions. The error bars for the vertical axis represent the measurement uncertainty from the energy-loss measurement. A linear increase of the target thickness with increasing back-pressure can be seen for all three ion projectiles. However, the linear fits to the data, especially for Ar, are in rather poor agreement with each other. This might be caused by a systematic error in the energy measurements or the uncertainties of the SRIM estimations. For the thickness calibration, comparing the measured charge state distributions, a mean value is used.

Measurements of the gas pressure in the gas cell, for increasing back-pressures on the valves, are shown in Fig. 4(c) for H_2 gas. The pressure in the gas cell was measured with the piezoelectric pressure gauge at the side of the gas cell (see Fig. 2). The uncertainties of this measurement are mainly caused by noise due to physical shock on the setup from the fast gas injection. In the applied back-pressure range, the pressure at the gas cell increases linearly.

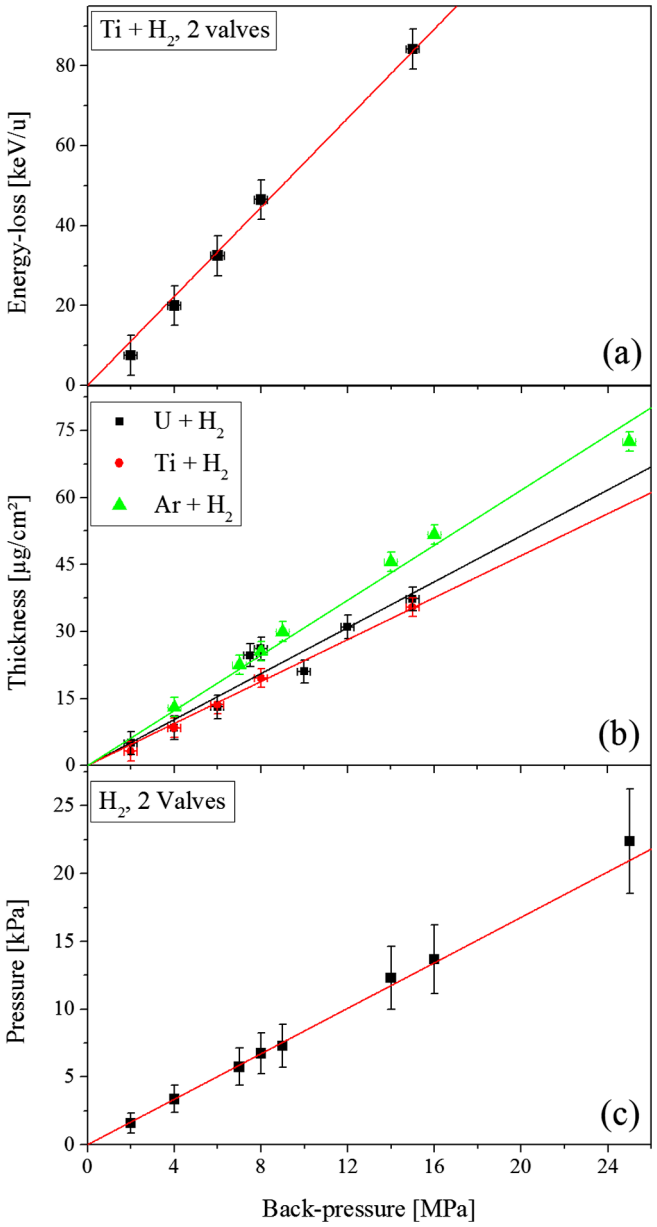

FIG. 4. (a) Energy-loss measurements for ^{50}Ti on H_2 gas at 1.4 MeV/u as a function of the back-pressure, using both gas valves. The red line represents a linear function fitted to the measurement data. (b) Estimated thickness of the H_2 gas target at 1.4 MeV/u depending on the back-pressure on the gas valves. The different lines represent linear functions fitted to the measurement data with corresponding equal color. (c) Pressure measurement using the piezoelectric pressure gauge near the interaction zone of the stripper with H_2 gas. The pressure increases linearly with increasing back-pressure on the valves. The red line represents a linear function fitted to the measurement data.

As both trends observed in the energy loss and pressure measurements are linear, it is assumed that the effective gas density in the gas cell is also increasing linearly with the back-pressure on the valves within the applied back-pressure range. As the setup is a windowless gas cell,

the gas is expected to be distributed along the beam line. From the conducted measurements, it is not possible to deduce the density distribution along the gas target. An estimation of the effective gas target length L was made using the measured pressure and obtained target thickness shown above, assuming the effective gas density to be constant along the beam line:

$$L = \frac{X}{\rho(P)}. \tag{7}$$

X denotes the target thickness and $\rho(P)$ the density of the H_2 gas depending on the pressure P, which is converted from the gas density of H_2 at normal conditions (89.9 g/m^3 at 1 bar). From this, a target length of about 35 mm is estimated, which seems reasonable compared to the length of the fitting enclosing the interaction zone of the gas cell, which is 44 mm. The corresponding effective gas density during the measurements is then in the order of 10 g/m^3 (10^{24} molecules/m^3), depending on the back-pressure on the valves.

III. EXPERIMENTAL RESULTS

A. Charge state distributions

Charge state distributions were measured, as described in Sec. II B, for ^{238}U, ^{209}Bi, ^{50}Ti, and ^{40}Ar ion beams at 0.74 MeV/u and 1.4 MeV/u beam energy passing through H_2, He, CO_2, N_2, O_2, Ne, and Ar gas targets for various target thicknesses. The systematic uncertainty of the charge state fractions is ±4% due to measurement uncertainties of the stripping efficiency. Additionally, a systematic error was observed at the charge state separation. At highest measured target thicknesses, the sum of the stripping efficiencies is reduced, dropping below 100%. The reduced total efficiency may be caused by a loss of ions before entering the charge state separation system due to increased angular straggling in the dense gas target. This effect would influence the charge state distributions in a similar way for all ion projectiles. Additionally, it is independent of the charge state of the ions. For the heavy projectiles ^{238}U and ^{209}Bi, reduced total transmission could be caused by an insufficient resolution of charge peaks of higher charge states (>30+) behind the dipole magnet. However, the charge peak resolution for ^{50}Ti and ^{40}Ar beams was sufficient to clearly separate all charge states for all applied target thicknesses. This effect is not included in the depicted error bars for the charge state fractions shown here.

1. Measurements at 1.4 MeV/u

In Fig. 5, the charge state distributions of ^{238}U, ^{209}Bi, ^{50}Ti, and ^{40}Ar ion beams at 1.4 MeV/u after passing through H_2 and He gas are shown. With increasing target thickness the charge state distributions shift to higher charge states. For ^{238}U on He (b), ^{50}Ti on H_2 (d), and ^{50}Ti on He (e), also the shape of the charge state distribution is changing for different target thicknesses. Beyond a certain threshold target thickness, the charge state distribution is saturated and does not significantly change anymore.

For some ion-target combinations, especially at low target thicknesses, the stripping efficiencies could not be measured for all charge states of the charge state distribution, as described in Sec. II B. Therefore, the normalization to obtain charge state fractions will not give accurate values. To obtain the missing stripping efficiencies, the distributions were fitted with a Gaussian function including a skewness correction, as used in [25]:

$$F_a(q) = F_C \cdot \exp\left(-\frac{t^2}{2(1+e_a t)}\right), \tag{8}$$

with

$$t = \frac{q - q_C}{\sigma}. \tag{9}$$

F_C denotes the maximum height of the distribution, q_C the charge state at the maximum height of the distribution, and σ the distribution width. e_a is a factor describing the asymmetry of the distribution. For a standard Gaussian function e_a is equal to zero.

For ^{238}U, ^{50}Ti, and ^{40}Ar on H_2 and He gas, the charge state fractions for all measured charge states plotted as a function of the target thickness are shown in Fig. 6. The charge state fractions reflect the behavior of the charge state distributions in Fig. 5. A saturation can be observed after passing a certain target thickness. At highest target thicknesses, the charge state fractions show again slight changes, e.g., for Ti on H_2 gas (b) and Ar on H_2 gas (c) in Fig. 6. This effect will be discussed in Sec. IV.

In Fig. 7, the charge state distributions of ^{238}U ion beams on O_2 as well as ^{209}Bi on He and Ar gas and ^{50}Ti on N_2 gas are shown. For these measurements, the energy-loss data were insufficient to provide a calibration to the target thickness. Therefore the charge state distributions are shown in dependency on the applied back-pressure on the pulsed gas valves. For ^{209}Bi on He gas [Fig. 7(b)], the applied back-pressure range was small and did not allow us to determine if saturation was reached.

For ^{238}U on N_2, CO_2, Ne, and Ar gas only measurements at high back-pressures, in the saturated charge state distribution regime were performed. This was inferred from the observation that the charge state distribution was not changing in the applied back-pressure range. The corresponding saturated charge state distributions are shown in Fig. 8. Missing charge state fractions were estimated using the fit described above, to show charge state fractions that can be compared to the other data.

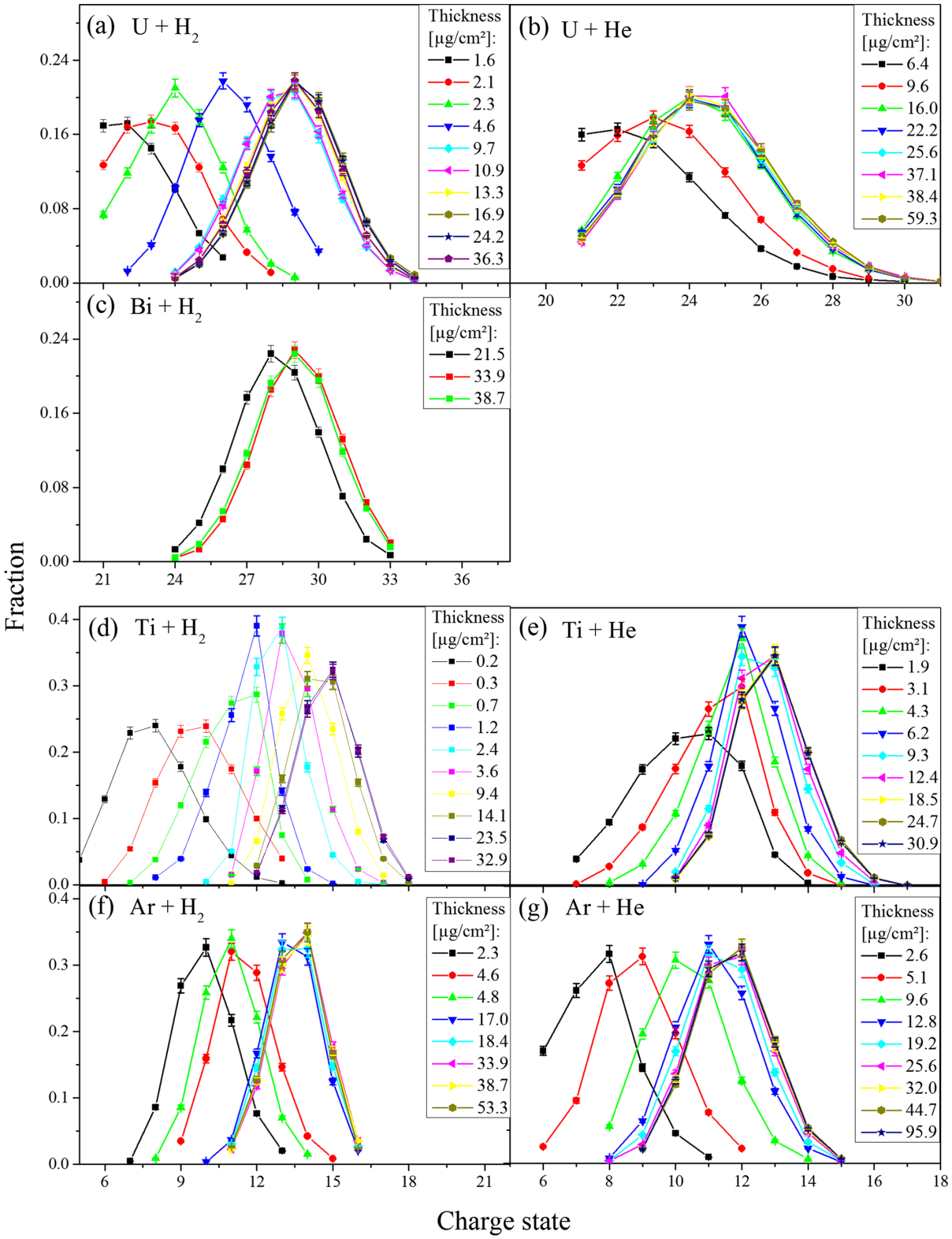

FIG. 5. Charge state distributions of ^{238}U, ^{209}Bi, ^{50}Ti, and ^{40}Ar ion beams at 1.4 MeV/u after passing through H_2 and He gas for various target thicknesses. The lines are added to guide the eye.

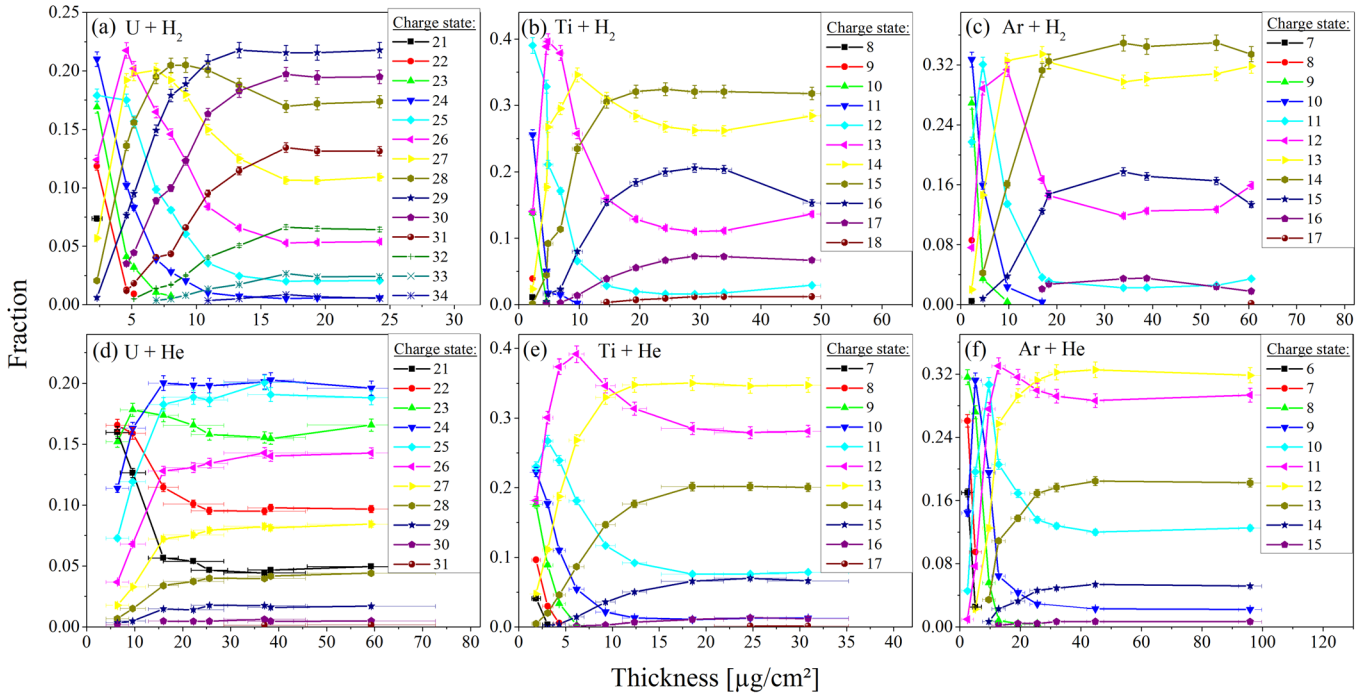

FIG. 6. Measured charge state fractions for ^{238}U, ^{50}Ti, and ^{40}Ar at 1.4 MeV/u on H_2 and He gas for increasing target thicknesses, corresponding to the charge state distributions shown in Fig. 5.

In Fig. 9, charge state fractions are shown for ^{238}U on O_2 gas depending on the back-pressure on the pulsed gas valves, corresponding to the charge state distributions shown in Fig. 7(a). At the back-pressure of 1 MPa, the charge state fractions reach saturation, before slightly changing again to lower charge states when going to highest target thicknesses. Charge state fractions were plotted only for ^{238}U on O_2 gas, because the other ion-target

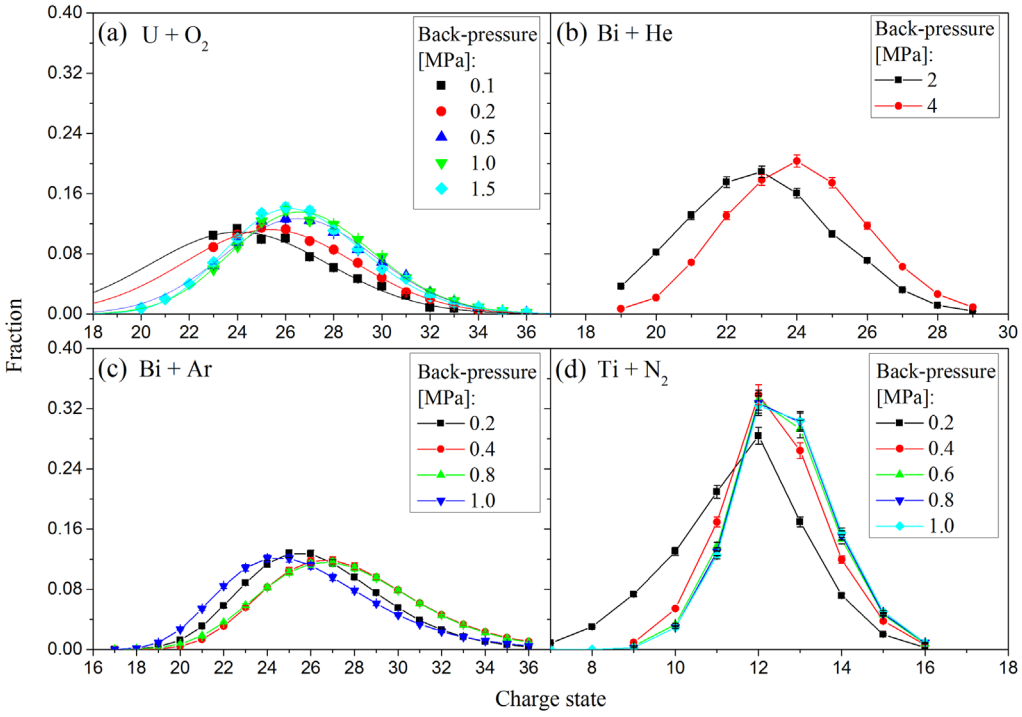

FIG. 7. Charge state distributions for ^{238}U on O_2 (a), ^{209}Bi on He (b), and Ar gas (c) as well as ^{50}Ti on N_2 gas (d) at 1.4 MeV/u for different back-pressures on the valve. For (a) and (c) the fit is shown, which was used to obtain missing charge fractions, as described in the text. For (b) and (d) lines were added to guide the eye.

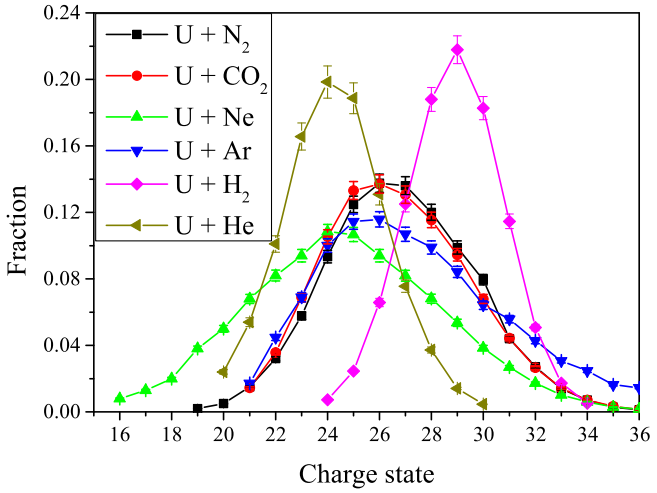

FIG. 8. Saturated charge state distributions for ^{238}U on N_2, CO_2, Ne, and Ar gas at 1.4 MeV/u. The saturated charge state distributions for ^{238}U on H_2 and He (see Fig. 5) are shown for comparison.

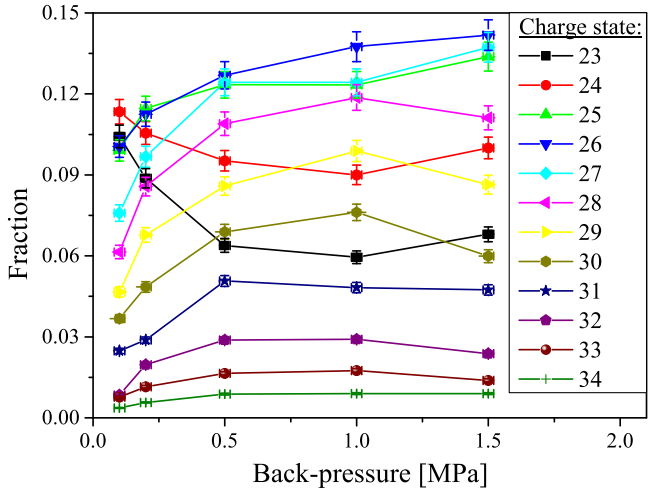

FIG. 9. Measured charge state fractions for ^{238}U on O_2 gas at 1.4 MeV/u, corresponding to the charge state distributions shown in Fig. 7(a).

combinations lacked a sufficient number of measurements before a saturated charge state distribution was achieved.

2. *Measurements at* 0.74 MeV/u

Measurements with ^{238}U and ^{50}Ti ions at 0.74 MeV/u were performed by turning off the rf-power of the second IH cavity of the HSI. The experimental setup behind the HSI remained unchanged. Due to the reduced beam energy the target thickness, required to achieve saturated charge state distributions, is reduced. Therefore, mostly saturated charge state distributions were measured in the applied range for the target thickness. This was verified by measuring the charge state distribution of each ion-target

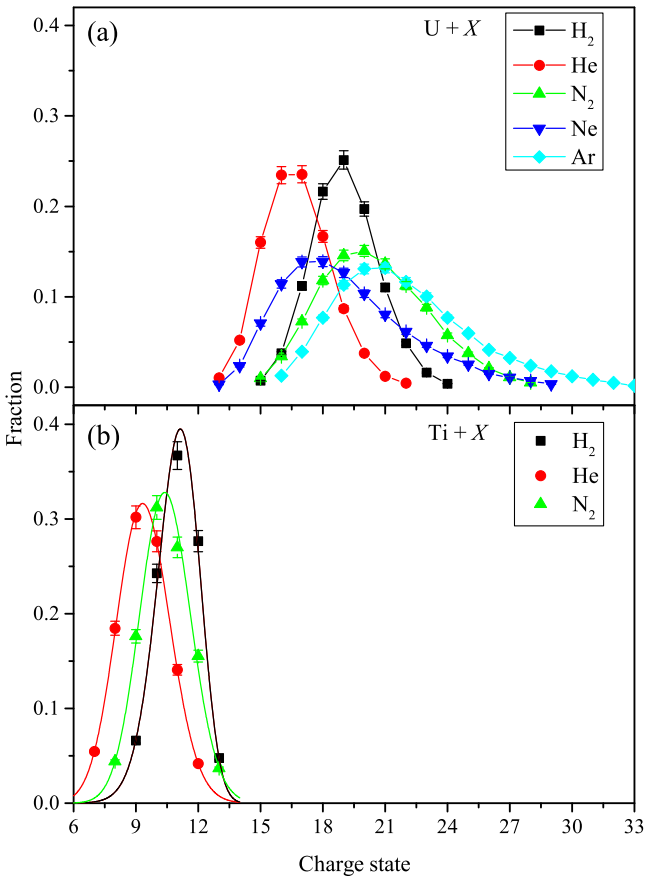

FIG. 10. Saturated charge state distributions for ^{238}U on H_2, He, N_2, Ne, and Ar gas (a) and ^{50}Ti on H_2, He, and N_2 gas (b) at 0.74 MeV/u beam energy.

combination for at least three different target thicknesses. In Fig. 10 the measured saturated charge state distributions are shown for ^{238}U on H_2, He, N_2, Ne, and Ar gas and ^{50}Ti on H_2, He, and N_2 gas. Compared to the measurements at 1.4 MeV/u the average charge states are reduced, as expected.

B. Mean charge state and distribution width

Using the charge state fractions shown above, the mean charge state $\bar{q}$ of the charge state distribution [9] can be obtained by:

$$\bar{q} = \sum_i F_{q_i} \cdot q_i. \tag{10}$$

In Fig. 11, $\bar{q}$ is plotted against the estimated target thickness for ^{238}U, ^{50}Ti, and ^{40}Ar ion beams at 1.4 MeV/u. A saturation is observed at transition to higher target thicknesses. Exponential fits were added for an improved distinguishable visibility at higher target thicknesses. For ion-target combinations where a thickness calibration could not be conducted, the saturated mean charge states (compare with Fig. 7 and Fig. 8) obtained from the

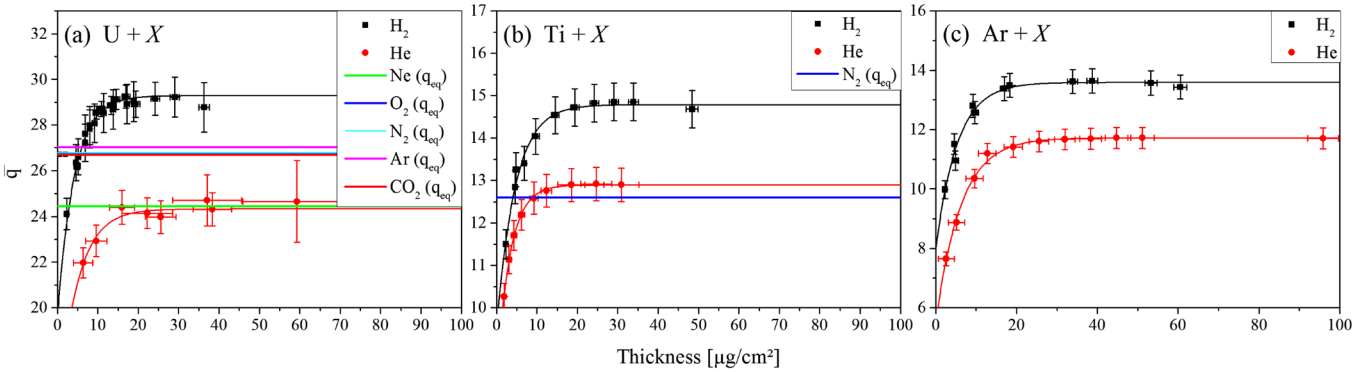

FIG. 11. Mean charge states $\bar{q}$ for ^{238}U (a), ^{50}Ti (b), and ^{40}Ar (c) ion beams at 1.4 MeV/u. Exponential fits are added to the data points to guide the eye. Saturated mean charge states, measured for ion-gas combinations without thickness estimation, are added as solid lines.

measurements are shown as a line. For ^{209}Bi ions, the data was insufficient to plot the mean charge states in this way.

The width d of the charge state distribution [9] is obtained by:

$$d = \left[\sum_{q_i}(q_i - \bar{q})^2 \cdot F_{q_i}\right]^{\frac{1}{2}}, \tag{11}$$

depicted for ^{238}U, ^{50}Ti, and ^{40}Ar ion beams on H_2 and He gas in Fig. 12. A saturation of the distribution width is observed with increasing target thickness.

IV. DISCUSSION

As described in Sec. III, saturation of the mean charge state could be measured for all ion-target combinations, except for ^{209}Bi on He gas. Before saturation the charge state fractions are rapidly changing (see Fig. 6 and 9) and the charge state distribution is shifting. The width of the charge state distribution reaches saturation at about the same target thickness as the mean charge state or is observed to be unchanged in the applied range for the target thickness. This can be seen when comparing the evolution of the mean charge state (Fig. 11) and the distribution width (Fig. 12) as a function of the target thickness for ^{238}U, ^{50}Ti, and ^{40}Ar ion beams on H_2 and He gas. For higher target thicknesses the charge state distribution does not change anymore. Therefore, it is assumed that a charge state equilibrium was reached.

For increasing target densities, the time between two successive collisions is decreasing. When this time interval becomes smaller than the lifetime of ions in an excited state, e.g., due to previous collisions, the probability that an electron is lost from the ion is increasing significantly. This is the so-called "density effect" and describes the change of cross sections for charge-changing processes in ion-atom collisions with increasing target densities [9,26]. As described in Sec. II C, it is not possible to make accurate predictions for the density distribution of the pulsed gas cell along the beamline. Only the effective target thickness can be estimated. Therefore, it is not attempted to make an estimate of the contribution of the density effect to the resulting equilibrated charge state distribution, as a sufficient description is beyond the scope of this paper.

For the charge state fractions of different ion-target combinations, a slight shift back toward lower charge states was observed when increasing the target thickness further. This has been observed, e.g., for ^{50}Ti and ^{40}Ar on

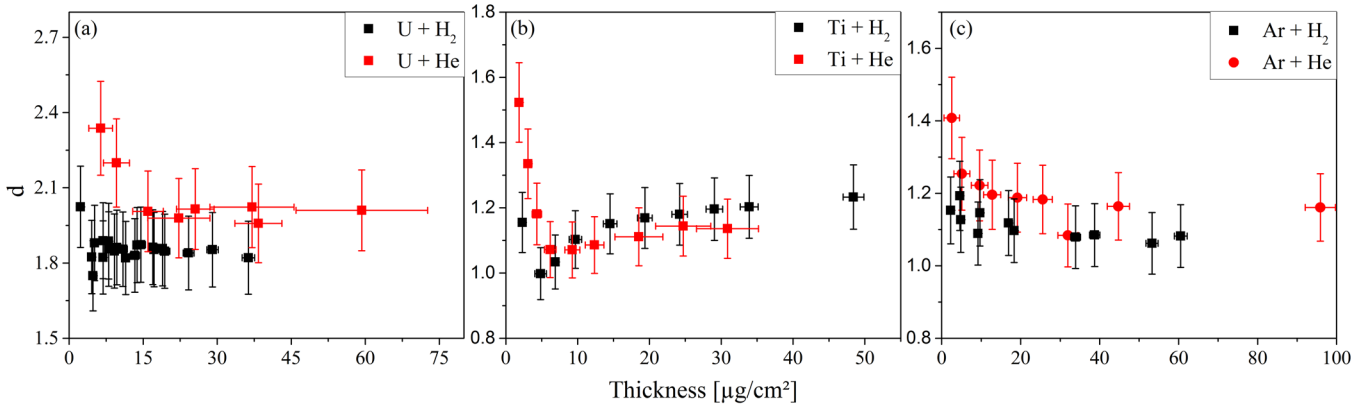

FIG. 12. Width d of the charge state distributions of ^{238}U (a), ^{50}Ti (b), and ^{40}Ar (c) ion beams on H_2 and He gas at 1.4 MeV/u.

H_2 gas [Fig. 5(b,c) and Fig. 6(b,c)]. The obtained energy loss for ^{50}Ti and ^{40}Ar ion beams for thicknesses of 32.9 μm/cm^2 and 53.3 μm/cm^2 is about 76 ± 5 keV/u and 100 ± 5 keV/u, respectively. The equilibrated mean charge state strongly depends on the ion energy (see, e.g., [27–29]). Therefore, this changes in the charge state fractions may be caused by the reduction in ion energy during the transition through the gas target when going to highest target thicknesses. Another possible reason is a broader distribution of the gas along the beamline by increasing the back-pressure on the gas valves, going to higher target thicknesses. If the ions are passing an extended area with a less dense gas when leaving the stripper, the equilibrium charge state is changing again.

The equilibrated mean charge state is of major interest for various applications, for example in gas-filled recoil separators, e.g., TASCA [30,31]. There, the aim is to make accurate predictions of the mean charge state of ions after passing a dilute gas, taking into account the density effect. For the accelerator-related application in gas strippers, the most abundantly populated charge state is of interest, as it allows for highest beam intensities. Additionally, high charge states are desired for the acceleration process to higher beam energies. In Table I, the obtained mean charge states $\bar{q}$ and the corresponding distribution widths d are shown for all measured ion-target combinations for which a charge state equilibrium was achieved. For H_2 gas at 1.4 MeV/u, the mean charge state is significantly increased compared to all other gas targets. A similar behavior was reported in [32] for ^{12}C ions at 2–10 MeV/u and in [33] for ^{127}I ions, where increased equilibrium charge states were measured for H_2 gas relative to He gas at an ion energy of 0.87 MeV/u.

We note that lower equilibrated mean charge states were observed for He and Ne, compared to the other gas targets, independent of the beam energy. This is probably caused by closed electron shells in the atomic structure, which result in strongly-bound electrons. A similar effect was described with the oscillation of equilibrium charge states with increasing nuclear charge of the target Z_T for Si and Cl ions [34] as well as in [9].

The behavior of the equilibrium charge state among the different gas targets changes at 0.74 MeV/u. The mean charge state for ^{238}U on H_2 gas is reduced, compared to N_2 and Ar gas. This is similar for ^{50}Ti on H_2 and N_2 gas. A shift of the equilibrium charge states of H_2, and also He, compared to heavier gas targets can also be seen in measurements at different ion energies. Measurements for ^{238}U ions at comparatively low ion energies (0.008 MeV/u–0.063 MeV/u), showed lower equilibrium charge states for H_2 and He gas compared to heavier gas targets [35]. At 10.8 MeV/u projectile energy, increased equilibrium charge states were measured for ^{238}U ions on H_2 and He gas, compared to N_2, Ne, and Ar gas [25,36]. This significant shift of the equilibrium charge states for low-Z gases at higher ion energies is not fully understood but may reflect the atomic structure of the target gas.

TABLE I. Mean charge states $\bar{q}$ and distribution widths d, obtained from the measurement data, and the calculated mean charge state $\bar{q}_{th}$. using the Schiwietz formula, as described in the text, for all ion-target combinations for which a charge state equilibrium was achieved.

Ion	Gas target	Energy (MeV/u)	$\bar{q}$	d	$\bar{q}_{th}$.
^{238}U	H_2	1.40	29.2 ± 1.2	1.8 ± 0.1	27.4
	He	1.40	24.3 ± 1.0	2.0 ± 0.1	27.7
	N_2	1.40	26.7 ± 1.1	3.7 ± 0.2	28.4
	O_2	1.40	26.5 ± 1.0	3.0 ± 0.2	28.4
	CO_2	1.40	26.7 ± 1.0	2.8 ± 0.2	28.4
	Ne	1.40	24.4 ± 1.0	3.6 ± 0.1	27.7
	Ar	1.40	25.8 ± 1.0	3.4 ± 0.1	28.9
^{209}Bi	H_2	1.40	29.2 ± 1.2	1.7 ± 0.1	26.1
	Ar	1.40	26.3 ± 1.1	3.6 ± 0.2	27.4
^{50}Ti	H_2	1.40	14.8 ± 0.6	1.1 ± 0.1	12.8
	He	1.40	12.9 ± 0.5	1.2 ± 0.1	12.8
	N_2	1.40	12.6 ± 0.5	1.2 ± 0.1	12.9
^{40}Ar	H_2	1.40	13.6 ± 0.5	1.1 ± 0.1	11.3
	He	1.40	11.7 ± 0.5	1.2 ± 0.1	11.3
^{238}U	H_2	0.74	19.1 ± 0.8	1.6 ± 0.1	19.5
	He	0.74	16.8 ± 0.7	1.6 ± 0.1	19.9
	N_2	0.74	20.5 ± 0.8	2.6 ± 0.1	20.4
	Ne	0.74	19.1 ± 0.8	3.1 ± 0.1	20.6
	Ar	0.74	21.9 ± 0.9	3.3 ± 0.1	20.9
^{50}Ti	H_2	0.74	11.0 ± 0.4	1.0 ± 0.1	9.9
	He	0.74	9.4 ± 0.4	1.2 ± 0.1	9.9
	N_2	0.74	10.4 ± 0.4	1.2 ± 0.1	10.1

Consequentially, the choice of the gas target for a charge stripper depends strongly on the beam energy, as the charge state behind the gas stripper has to be matched with the injection threshold of the adjacent accelerator structures. Additionally, higher charge states behind the stripper enable a reduced rf power consumption for adjacent accelerator structures. With an increased mean charge state of the charge state distribution, this becomes possible without a loss of efficiency. However, for high beam-intensity applications the benefit must be balanced against the increase of space charge effects scaling with q^2.

The mean charge state can be predicted with semi-empirical formulas, e.g., by Schiwietz and Grande [37]. In this approach, the mean charge state $\bar{q}_{th}$ is estimated by

$$\bar{q}_{th} = Z_P \cdot \frac{376x + x^6}{1428 - 1206x^{0.5} + 690x + x^6}, \quad (12)$$

with the scaling parameter

$$x = \left(v_p/v_0 \cdot Z_P^{-0.52} Z_T^{0.03-0.017 \cdot Z_P^{-0.52} \cdot v_P/v_0} \right)^{1+0.4/Z_P}. \quad (13)$$

Z_P and Z_T denote the atomic charge of the projectile ion and the target atom, respectively. v_P is the velocity of the

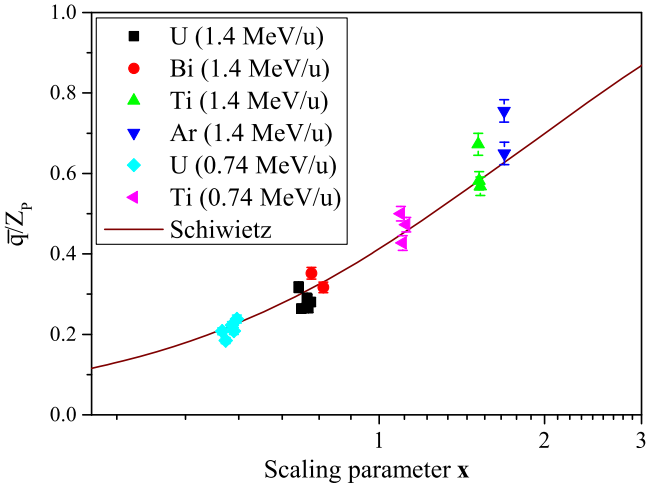

FIG. 13. Measured data plotted as ratio of the mean charge state to the atomic charge of the projectile ion against the scaling factor x, as described in the text, and compared to estimations by the Schiwietz formula [37].

projectile ion, and v_0 is the Bohr velocity ($v_0 = 2.19 \times 10^6$ m/s). Estimated mean charge states $\bar{q}_{th}$ for ion-target combinations measured in this work are shown in Table I. A graphical comparison with the measurement data listed in Table I is shown in Fig. 13. The formula generally describes the mean charge state of the measured ions at both ion energies. For H_2 gas, except for ^{238}U at 0.74 MeV/u, the estimated equilibrium charge states are lower compared to the measurements (see Table I), with a maximum discrepancy of 17%. The formula estimates slightly reduced equilibrium charge states for He and Ne at both ion energies compared to all other gases, which was also observed in the measurements. In general, the values estimated by the formula describe a different behavior of the mean charge state depending on Z_T, compared to the measurements.

For the heaviest projectiles, ^{238}U and ^{209}Bi, the shape of the charge state distribution becomes broader and asymmetric after passing heavier gas targets. This is shown in Fig. 7(c) for ^{209}Bi on Ar gas, Fig. 8 for ^{238}U on Ar gas, and also for the equilibrated charge state distributions in Table I for all applied gas targets. This behavior is known for charge state distributions of ions passing through heavy gas targets, as described in [9,38]. It is caused by an increasing contribution of so-called "multi-electron processes" in the charge-changing collisions. In these processes, more than one electron is lost or captured by the ion. The cross sections for multi-electron loss are increasing for higher Z_T. By using low-Z gases like H_2 and He for stripping of ^{238}U and ^{209}Bi, the cross sections for multi-electron processes are decreased and narrower charge state distributions result (see Fig. 8). This effect was also observed in [25], measuring the distribution width of ^{86}Kr on H_2, He, and N_2 gas. Due to the narrow charge state distributions, the charge state fractions of the populated charge states are increased. Therefore, the use of H_2 and He gas enables for increased stripping efficiencies and, thus, increased beam intensities behind the gas stripper when utilizing these charge states.

For broader charge state distributions the charge state fractions are more widely distributed around the mean charge state as the average number of collision-transferred electrons increases. Additionally, the contribution of multi-electron processes on the total cross sections vary depending on the charge state of the ion, different to single-electron processes. The resulting increased charge state fractions at higher charge states are accountable for forming the elevated tail in the otherwise Gaussian-shaped charge state distributions [see, e.g., Fig. 7(c)]. For the charge state distributions of ^{50}Ti and ^{40}Ar ions, an equally significant effect on the shape of the charge state distribution was not observed. A possible reason could be the lower number of electrons in the atomic shell of the projectile, resulting in reduced cross sections for multi-electron processes. Therefore, the charge state distribution becomes more narrow as the average number of electrons, transferred in charge-exchanging processes, is decreasing.

A sudden shift in the shape of the charge state distribution at higher target thicknesses were observed for ^{50}Ti on H_2 and He gas (Fig. 5d,e). This effect is caused by so-called "shell effects" [39]. The cross sections of charge-changing processes change significantly when the ionization energy of ion changes. For ^{50}Ti, this is seen in the transition from charge state 12 to 13 in the change of the shape of the charge state distribution and the change of the distribution width [see Fig. 5 and Fig. 12(b)]. The distribution width increases again after reaching a minimum at the target thickness corresponding to the stated charge state transition. After losing 12 electrons the Ti ion has the electron configuration $1s^2 2s^2 2p^6 3s^0 3p^0 3d^0 4s^0$, a magic number of remaining electrons, and, therefore, has strongly-bound outer electrons. The ionization energy of Ti^{12+} is 787.67 ± 0.04 eV compared to 291.5 ± 0.005 eV for Ti^{11+} [40]. For ^{238}U a less significant shell effect can be seen at the transition from charge state 24 to 25 [see Fig. 5(a) and Fig. 12(a)]. ^{209}Bi and ^{40}Ar do not have a shell transition in the measured charge state range. Similar observations were reported in [33,36,41]. The ionization energy of the ion when passing through gas has to be taken into account when calculating charge-changing cross sections (see, e.g., [31]). These shell effects can be utilized to acquire increased beam intensities behind the gas stripper, especially for ion beams, where a high charge state is not essential for further acceleration due to a low Z_P or a desired, reduced final beam energy, e.g., for ^{50}Ti projectiles.

For the application in accelerators it is important to note that an increased target thickness affects the ion-beam energy, as mentioned above, as well as the beam emittance. The ion-beam energy is an important parameter for the

injection of the beam into the adjacent accelerator structures, like the Alvarez DTL accelerator [11] at the GSI UNILAC. Therefore, the energy loss in the pulsed gas stripper cell has to be taken into account when increasing the applied target thickness. The beam emittance is a crucial parameter for the accelerator performance and is influenced by the angular straggling of the ions in the gas target as well as increased space charge forces due to charge stripping. However, the behavior of the beam emittance for ion beams passing the pulsed gas stripper cell is not discussed here. Previous works have already reported on this [16,19].

V. CONCLUSION

The charge state distributions for ^{238}U, ^{209}Bi, ^{50}Ti, and ^{40}Ar ions at 0.74 MeV/u and 1.4 MeV/u beam energy passing through H_2, He, CO_2, N_2, O_2, Ne, and Ar gas have been measured for target thicknesses in the range of $\leq 100\ \mu g/cm^2$. Measured charge state distributions, including mean charge states and distribution widths, are presented. For most ion-target combinations a charge state equilibrium was reached. The observed behaviors, including broadening of the distribution and shell-effects, and their importance for gas stripper applications have been discussed. At 1.4 MeV/u, the use of H_2 gas results in increased mean charge states for all used ion projectiles. H_2 and He gas targets provide for more narrow charge state distributions compared to heavier gases and, thereby, enable increased beam intensities behind the stripper.

ACKNOWLEDGMENTS

The authors are grateful for the support of the GSI linac, ion source, linac-rf, technical infrastructure and accelerator operation departments and operators from other GSI departments.

[1] Y. Yano, The RIKEN RI Beam Factory Project: A status report, Nucl. Instrum. Methods Phys. Res., Sect. B **261**, 1009 (2007).

[2] J. Wei *et al.*, FRIB accelerator status and challenges, in *Proceedings of LINAC2012, Tel-Aviv, Israel* (JACoW, Geneva, 2012), Vol. 12, pp. 417–421.

[3] J. Yang, J. Xia, G. Xiao, H. Xu, H. Zhao, X. Zhou, X. Ma, Y. He, L. Ma, D. Gao *et al.*, High Intensity heavy ion Accelerator Facility (HIAF) in China, Nucl. Instrum. Methods Phys. Res., Sect. B **317**, 263 (2013).

[4] O. Kester *et al.*, Status of the FAIR facility, in *Proceedings of the 4th International Particle Accelerator Conference, IPAC-2013, Shanghai, China, 2013* (JACoW, Shanghai, China, 2013).

[5] J. Ziegler, SRIM–The Stopping and Range of Ions in Matter, see http://www.srim.org (2013).

[6] W. Barth, M. S. Kaiser, B. Lommel, M. Maier, S. Mickat, B. Schlitt, J. Steiner, M. Tomut, and H. Vormann, Carbon stripper foils for high current heavy ion operation, J. Radioanal. Nucl. Chem. **299**, 1047 (2014).

[7] F. Marti *et al.*, Heavy ion strippers, in *Proceedings of LINAC2012, Tel-Aviv, Israel* (JACoW, Geneva, 2012), pp. 1050–1054.

[8] N. Bohr, Scattering and stopping of fission fragments, Phys. Rev. **58**, 654 (1940).

[9] H. D. Betz, Charge states and charge-changing cross sections of fast heavy ions penetrating through gaseous and solid media, Rev. Mod. Phys. **44**, 465 (1972).

[10] W. Barth and P. Forck, The new gas stripper and charge state separator of the GSI high current injector, arXiv: physics/0008088.

[11] L. Groening, A. Adonin, M. Baschke, X. Du, Ch. E. Düllmann, R. Hollinger, H. Hähnel, E. Jäger, M. Maier, S. Mickat *et al.*, Upgrade of the universal linear accelerator UNILAC for FAIR, in *Proceedings of IPAC2016, Busan, Korea* (JACoW, Geneva, 2016) p. 880.

[12] P. Scharrer, E. Jäger, W. Barth, M. Bevcic, Ch. E. Düllmann, L. Groening, K. P. Horn, J. Khuyagbaatar, J. Krier, and A. Yakushev, Electron stripping of Bi ions using a modified 1.4 MeV/u gas stripper with pulsed gas injection, J. Radioanal. Nucl. Chem. **305**, 837 (2015).

[13] V. Shevelko, N. Winckler, and I. Y. Tolstikhina, Gas-pressure dependence of charge-state fractions and mean charges of 1.4 MeV/u-uranium ions stripped in molecular hydrogen, Nucl. Instrum. Methods Phys. Res., Sect. B **377**, 77 (2016).

[14] H. Imao, H. Okuno, H. Kuboki, S. Yokouchi, N. Fukunishi, O. Kamigaito, H. Hasebe, T. Watanabe, M. Kase, and Y. Yano, Charge stripping of uranium-238 ion beam with low-Z gas stripper, in *Proceedings of the 2nd International Particle Accelerator Conference, San Sebastiáán, Spain* (EPS-AG, Spain, 2011).

[15] P. Scharrer, W. Barth, M. Bevcic, Ch. E. Düllmann, L. Groening, K. Horn, E. Jäger, J. Khuyagbaatar, J. Krier, and A. Yakushev, Stripping of high intensity heavy-ion beams in a pulsed gas stripper device at 1.4 MeV/u, in *Proceedings of IPAC2015, Richmond, VA, USA* (JACoW, Geneva, 2015).

[16] W. Barth, A. Adonin, Ch. E. Düllmann, M. Heilmann, R. Hollinger, E. Jäger, J. Khuyagbaatar, J. Krier, P. Scharrer, H. Vormann *et al.*, U^{28+}-intensity record applying a H_2-gas stripper cell, Phys. Rev. ST Accel. Beams **18**, 040101 (2015).

[17] P. Scharrer, W. Barth, M. Bevcic, Ch. E. Düllmann, L. Groening, K. Horn, E. Jäger, J. Khuyagbaatar, J. Krier, and A. Yakushev, A pulsed gas stripper for stripping of high-intensity, heavy-ion beams at 1.4 MeV/u at the GSI UNILAC, in *Proceedings of HIAT2015, Yokohama, Japan* (JACoW, Geneva, 2015).

[18] P. Scharrer, W. Barth, M. Bevcic, Ch. E. Düllmann, L. Groening, K. Horn, E. Jäger, J. Khuyagbaatar, J. Krier, and A. Yakushev, An upgrade for the 1.4 MeV/u gas stripper at the GSI UNILAC, in *Proceedings of IPAC2016, Busan, South Korea* (JACoW, Geneva, 2016).

[19] P. Scharrer, W. Barth, M. Bevcic, Ch. E. Düllmann, L. Groening, K. Horn, E. Jäger, J. Khuyagbaatar, J. Krier, and A. Yakushev, Developments on the 1.4 MeV/u pulsed

gas stripper cell, in *Proceedings of LINAC2016, East Lansing, MI, USA* (JACoW, Geneva, 2016).

[20] GSI ion sources, https://www.gsi.de/en/work/organisation/divisions/beschleunigerbetrieb/ion_sources/sources/ion_sources.htm, accessed: 2016-09-15.

[21] R. Hollinger, M. Galonska, B. Gutermuth, F. Heymach, H. Krichbaum, K.-D. Leible, K. Ochs, P. Schäffer, S. Schäffer, P. Spädtke, M. Stork, A. Wesp, and R. Mayr, Status of high current ion source operation at the GSI accelerator facility, Rev. Sci. Instrum. **79**, 02C703 (2008).

[22] W. Barth, Commissioning of the 1.4 Mev/u high current heavy ion linac at GSI, arXiv:physics/0008087.

[23] W. Barth, W. Bayer, L. Dahl, P. Gerhard, L. Groening, and S. Yaramishev, GSI Scientific Report, 2006, p. 79.

[24] P. Scharrer, E. Jäger, W. Barth, M. Bevcic, Ch. E. Düllmann, L. Groening, K. P. Horn, J. Khuyagbaatar, J. Krier, and A. Yakushev (to be published).

[25] H. Kuboki, H. Okuno, H. Hasebe, N. Fukunishi, E. Ikezawa, H. Imao, O. Kamigaito, and M. Kase, Charge state distribution of ^{86}Kr in hydrogen and helium gas charge strippers at 2.7 MeV/nucleon, Phys. Rev. ST Accel. Beams **17**, 123501 (2014).

[26] J. Neufeld and W. Snyder, Dependence of the average charge of an ion on the density of the surrounding medium, Phys. Rev. **107**, 96 (1957).

[27] A. B. Wittkower and H. D. Betz, Equilibrium charge-state distributions of 2–15-MeV tantalum and uranium ions stripped in gases and solids, Phys. Rev. A **7**, 159 (1973).

[28] E. Baron, M. Bajard, and C. Ricaud, Charge exchange of very heavy ions in carbon foils and in the residual gas of GANIL cyclotrons, Nucl. Instrum. Methods Phys. Res., Sect. A **328**, 177 (1993).

[29] A. Perumal, V. Horvat, R. Watson, Y. Peng, and K. Fruchey, Cross sections for charge change in argon and equilibrium charge states of 3.5 MeV/amu uranium ions passing through argon and carbon targets, Nucl. Instrum. Methods Phys. Res., Sect. B **227**, 251 (2005).

[30] J. Khuyagbaatar, D. Ackermann, L.-L. Andersson, J. Ballof, W. Brüchle, Ch. E. Düllmann, J. Dvorak, K. Eberhardt, J. Even, A. Gorshkov *et al.*, Study of the average charge states of ^{188}Pb and ^{252,254}No ions at the gas-filled separator TASCA, Nucl. Instrum. Methods Phys. Res., Sect. A **689**, 40 (2012).

[31] J. Khuyagbaatar, V. P. Shevelko, A. Borschevsky, Ch. E. Düllmann, I. Yu. Tolstikhina, and A. Yakushev, Average charge states of heavy and superheavy ions passing through a rarified gas: Theory and experiment, Phys. Rev. A **88**, 042703 (2013).

[32] F. W. Martin, Equilibrium charge-state populations of carbon ions from 2 to 10 MeV/amu in H_2, N_2, Ar, and Ni, Phys. Rev. **140**, A75 (1965).

[33] S. Datz, C. D. Moak, H. O. Lutz, L. C. Northcliffe, and L. B. Bridwell, Charge states of 15–140 MeV bromine ions and 15–162 MeV iodine ions in solid and gaseous media, At. Data Nucl. Data Tables **2**, 273 (1970).

[34] K. Shima, T. Ishihara, T. Momoi, T. Miyoshi, K. Numata, and T. Mikumo, Z_2 oscillation of mean charge states of fast Si and Cl ions after passage through thin foils, Phys. Lett. **98A**, 106 (1983).

[35] A. B. Wittkower and H. D. Betz, Equilibrium charge-state distributions of 2–15-MeV tantalum and uranium ions stripped in gases and solids, Phys. Rev. A **7**, 159 (1973).

[36] H. Imao, H. Okuno, H. Kuboki, S. Yokouchi, N. Fukunishi, O. Kamigaito, H. Hasebe, T. Watanabe, Y. Watanabe, M. Kase *et al.*, Charge stripping of ^{238}U ion beam by helium gas stripper, Phys. Rev. ST Accel. Beams **15**, 123501 (2012).

[37] G. Schiwietz and P. Grande, Improved charge-state formulas, Nucl. Instrum. Methods Phys. Res., Sect. B **175**, 125 (2001).

[38] S. Datz, H. O. Lutz, L. B. Bridwell, C. D. Moak, H. D. Betz, and L. D. Ellsworth, Electron capture and loss cross sections of fast bromine ions in gases, Phys. Rev. A **2**, 430 (1970).

[39] C. D. Moak, H. O. Lutz, L. Bridwell, L. Northcliffe, and S. Datz, Evidence of Shell Effects and the Approach to Equilibrium in the Charge-State Distributions for 15–160 MeV ^{79}Br and ^{127}I Ions in Carbon, Phys. Rev. Lett. **18**, 41 (1967).

[40] NIST Atomic Spectra Database, http://www.nist.gov/pml/data/asd.cfm, accessed: 2016-09-17.

[41] A. Leon, S. Melki, D. Lisfi, J. Grandin, P. Jardin, M. Suraud, and A. Cassimi, Charge state distributions of swift heavy ions behind various solid targets ($36 < Z_p < 92$, 18 MeV/u $<$ E $<$ 44 MeV/u), At. Data Nucl. Data Tables **69**, 217 (1998).